Journal of Manufacturing Processes 68 (2021) 1824–1836

Contents lists available at ScienceDirect

Journal of Manufacturing Processes

journal homepage: www.elsevier.com/locate/manpro

Combination of structured light scanning and external fiducials for coordinate system transfer in hybrid manufacturing

Aaron Cornelius [a], Jake Dvorak [a], Leah Jacobs [a], Joshua Penney [a], Tony Schmitz [a,b,*]

[a] University of Tennessee, Mechanical, Aerospace, and Biomedical Engineering Department, Knoxville, TN, United States of America
[b] Oak Ridge National Laboratory, Manufacturing Science Division, Oak Ridge, TN, United States of America

ARTICLE INFO

Keywords:
Additive manufacturing
Milling
Structured light scanning
Metrology

ABSTRACT

This paper describes a method for establishing and transferring coordinate systems through multiple hybrid manufacturing operations. To demonstrate the approach, an additively manufactured preform is finish machined to produce the desired part geometry. A set of external fiducials is temporarily attached to the preform using a polymer frame. The assembly is inspected using a structured light scanner and the resulting scan is used to define an alignment and coordinate system which respects the physical requirements of the manufacturing processes. The coordinate system is then used to program subsequent machining operations. Once the part is set up on the milling machine, the fiducials are used to establish the shared coordinate system for the machining operation using standard on-machine probing. After the part is machined, the same fiducial/scanning process is repeated for a second machining operation to complete the part (i.e., some features could not be accessed in the first setup). Finally, the method performance is assessed.

1. Introduction

Hybrid manufacturing strategies are receiving increased attention, both in research and production, due to their ability to combine metal deposition with machining to produce complex part geometries with the required surface finish and geometric accuracy. The deposition and machining steps can occur in series or iteratively on a single machine or on separate machine tools. A persistent challenge in all cases is identifying the printed part geometry in the machining work coordinate system (WCS), or identifying the partially machined part geometry in the printing coordinate system for iterative approaches. Primary issues when establishing the shared coordinate systems include: 1) the non-prismatic geometries which are often implemented in additive designs to limit part count and minimize material use; and 2) variations in the printed part geometry and surface finish inherent to additive processes. The former makes datum identification difficult. The latter affects the actual radial and axial depths of cut during machining, which in turn, affect the machining stability and accuracy [1].

In this paper, the printed part geometry (preform) is measured by structured light scanning and the subsequent digital representation is used as the stock model for the computer-aided manufacturing (CAM) toolpath generation. The innovation is the inclusion of fiducials (precision spheres) and scanning targets that are located within the scan volume, but off the printed part. The fiducials and targets are mounted on a fused filament fabrication (FFF) polymer frame that is attached to the preform base plate. The fiducials enable the coordinate system definition, while the targets support the structured light scanning process. The process steps are detailed for a selected part, including measuring the preform geometry together with the fiducials and targets, identifying the optimal position of the computer-aided design (CAD) geometry within the preform, establishing the WCS by locating the precision spheres using the spindle-mounted probe, applying the WCS in the machining operations, repeating the process for two different machining setups on the same part (two setups were required to provide access to all part features using the three-axis milling machine), and evaluating the results. Conclusions and next steps are finally discussed.

2. Prior research

This project applies structured light scanning as the metrology instrument to simultaneously measure preform geometry and fiducials (precision spheres) in order to transfer the coordinate frame from the deposition to machining steps. Therefore, background information on hybrid manufacturing, structured light scanning, and fiducial markers is

* Corresponding author at: University of Tennessee, Mechanical, Aerospace, and Biomedical Engineering Department, Knoxville, TN, United States of America.
E-mail address: tony.schmitz@utk.edu (T. Schmitz).

https://doi.org/10.1016/j.jmapro.2021.07.011
Received 9 April 2021; Received in revised form 24 June 2021; Accepted 1 July 2021

provided for the interested reader.

2.1. Hybrid manufacturing

Webster et al. recently defined hybrid manufacturing as an "in-situ or series combination of an additive manufacturing process and secondary energy sources in which physical mechanisms are fundamentally altered/controlled to affect the resulting properties of the material and/or part" [2]. They describe the relationships between mechanical properties; physical mechanisms, such as melt pool dynamics and thermal gradients; energy source; and the associated hybrid manufacturing process, including AM + X processes, where X (e.g., milling) is used to provide the required surface finish and geometry. Several authors have reported strategies to implement AM + machining processes.

Liou et al. described the combination of powder-based laser metal deposition and computer numerically controlled (CNC) milling in a single machine [3]. They defined an automated process planning sequence composed of determining the base face (which functioned as the machining fixture), extracting the part skeleton, decomposing a part into subparts, determining build sequence and direction for subparts, checking the feasibility of the build sequence and direction for the machining process, and optimization of the deposition and machining steps. Yamazaki described the combination of laser metal deposition, turning, and milling capabilities in a single, commercial machine [4]. Advantages were increased functionality and flexibility for small lot production runs. Disadvantages include heat transfer into the machine structure from the laser deposition, which can limit accuracy, and the combination of powder (for deposition) and coolant (for machining) in the same work volume.

Chen discussed the capabilities of hybrid manufacturing while considering issues with CAD, computer-aided process planning (CAPP), and CAM for automated process planning [5]. Similarly, Waldschmidt et al. described an automated post-processing method for additively manufactured preforms [6]. The focus was specification of the clamping arrangement required by the printed part geometry and an automated CAM process planning method for three-axis milling operations.

2.2. Structured light scanning

A structured light scanning system is composed of a projector, which shines the selected structured pattern onto the test object, and one or more cameras then capture(s) the reflected, distorted pattern (caused by the object shape). The object shape is identified by analyzing the distortion after the system is calibrated and the spatial relationship between the projector and camera(s) is known. It has become a well-established instrument for manufacturing environment measurements.

As with any metrology system, the accuracy of structured light scanning systems has been assessed using various artifacts. Bernal et al. performed structured light scanning measurements of a calibration plate and gauge blocks with different sizes [7]. Key factors that were identified included the object and scanner temperature, optical characteristics of the object, vibrations during data collection, object orientation, number of images, and data analysis. Martínez-Pellitero et al. used an artifact composed of cylinders, spheres, and prismatic volumes to evaluate the performance of structured light scanners [8]. The artifact reference measurements were provided by a coordinate measuring machine (CMM). Ghandali et al. presented an artifact that includes vertically stacked 2D sphere plates with spacers and kinematic couplings to enable repeatable assembly [9]. The design created a 3D lattice that was measured to determine not only the distance between the centers of sphere pairs, but also the sphere sizes and forms. CMM measurements were compared to measurements performed using a structured light scanner. Mendricky used an artifact composed of multiple precision spheres with different diameters located in a single plane to evaluate structured light scanning performance [10]. McCarthy et al. described an aluminum alloy freeform artifact that was used to complete a measurement comparison between a CMM and three optical systems, including laser triangulation scanning, photogrammetry, and structured light projection [11]. Acko et al. tested tetrahedron-based artifacts for evaluating the measurement performance of optical 3D devices [12]. Moroni et al. described artifact-based evaluation of 3D optical measuring instruments that include a rotational axis. The artifacts were composed of a base plate with spheres positioned at different distances and heights. The artifacts were calibrated and then used to determine length measurement errors and axis of rotation errors [13].

2.3. Fiducial markers

Fiducial markers are routinely used in measurement applications. Their implementation spans the medical, microelectronics, and manufacturing fields. In medical applications for tumor treatment, fiducial markers are multi-millimeter-scale metal (typically gold) spheres, coils, or cylinders that are placed in or near a tumor to guide the radiation placement [14]. Naidu et al. applied endoscopic ultrasound-guided fiducial placement to compensate for tumor motion during respiration by tracking and determining tumor boundaries during stereotactic body radiotherapy [15]. Khullar et al. studied ultrasound techniques during fiducial marker deployment to mitigate the risk of marker migration and potential organ injury. This supported computed tomography-guided fiducial marker placement that is used to improve the accuracy of radiation treatment for liver tumors [16]. Ohta et al. used a gold fiducial marker to reduce treatment margins in external beam radiotherapy for prostate cancer by tracking interfraction motion. The marker's coiled shape was designed to avoid migration [17].

In other medical applications, Korte et al. used fiducial markers during robotic path planning training for surgery. The marker positions were recorded during procedure attempts and used to orient the recorded path relative to the patient's anatomy [18]. Also, Unkovskiy et al. used a handheld structured light scanner to measure auricles (visible portion of the external ear) with polymer fiducial spheres attached. The scanned digital model was then printed using FFF, selective laser sintering (SLS), and stereolithography (SL). Measurements of the in vivo, digital model, FFF, SLS, and SL auricles were compared using the fiducial spacing [19].

In printed circuit board (PCB) design, round copper markers are used as reference points for pick and place assembly. The markers enable pick and place machines to identify the PCB orientation and its surface mount components [20].

For manufacturing, fiducials have been used to provide machine calibration and part location capabilities. Smith et al. demonstrated the fiducial calibration system (FCS) with the intent to transfer the accuracy of a coordinate measuring machine to the shop floor for high-speed machining. In this approach, fiducials were attached to the large, monolithic workpiece and measured in a metrology environment. They were then remeasured in the manufacturing environment. A transformation was performed on the CNC program to alter the original programmed coordinates such that the machined features were correct regardless of the manufacturing environment and/or machine tool errors [21–22]. Wang et al. described the similar fiducial-aided calibration and positioning (FACP) concept. In this approach, the measured fiducials locations in the machining environment were fit to the positions of the fiducials in the CAD environment, which was obtained using a separate measuring instrument such as a coordinate measuring machine. The intent was to calibrate the cumulative errors and compensate by modifying the tool path [23].

Similar strategies have been implemented in additive manufacturing. Ferrucci et al. used inclined, cylindrical protrusions as reference fiducials in the design of cylindrical additively manufactured test coupons. Their intent was to align ex situ inspection data to a part's build geometry [24]. Boulger et al. used fiducials to locate layered surfaces on additively manufacturing polymer structures using a laser

tracker. This provided the ability to monitor the structure during fabrication and assess the part health [25]. Mathur et al. recently proposed an augmented reality (AR) framework and smartphone app as an alternative to conventional inspection for additively manufactured parts using integrated markers. The minimum fiducial pattern size produced by the deposition process that yielded the highest number of detectable features was studied [26].

This paper builds on these prior efforts by evaluating a method for establishing and transferring coordinate systems between hybrid manufacturing operations. The steps followed in this study are:

1. an aluminum preform is produced using additive manufacturing
2. a set of external fiducials is temporarily attached to the preform using a polymer frame
3. the assembly is measured using structured light scanning
4. the scan is used to define an alignment and coordinate system
5. the coordinate system is used to program machining operations for two orientations (top and bottom of the preform)
6. the fiducials are used to establish the machining coordinate system using standard on-machine probing
7. the preform is finish machined in two operations (top and bottom features).

3. Initial scanning

The aluminum alloy preform was manufactured by MELD Manufacturing Corporation using their solid-state additive process. The preform and the desired final geometry are shown in Fig. 1. Due to the internal geometry, this preform must be machined from both sides to produce the finished part.

The preform was first scanned to evaluate its accuracy and ensure that the nominal part design was contained within the preform. This was required to confirm it is possible to produce the desired geometry from the preform solely by removing material. Preform measurements were performed with a GOM ATOS Q structured light scanner. Ten scans were performed at different angles around the part so that the full geometry was captured.

The GOMInspect software was used to stitch the individual scans into a single mesh. The CAD model of the target part was imported and manually positioned relative to the scanned model to validate that the part was contained inside of the preform, as shown in Fig. 2. This step is referred to as an alignment.

While it may be confirmed that the CAD model is contained within the preform, this is not sufficient to guarantee that the final part geometry can be machined from the preform. In order to ensure that the part can actually be made from the preform, an alignment must be found which satisfies the following three criteria:

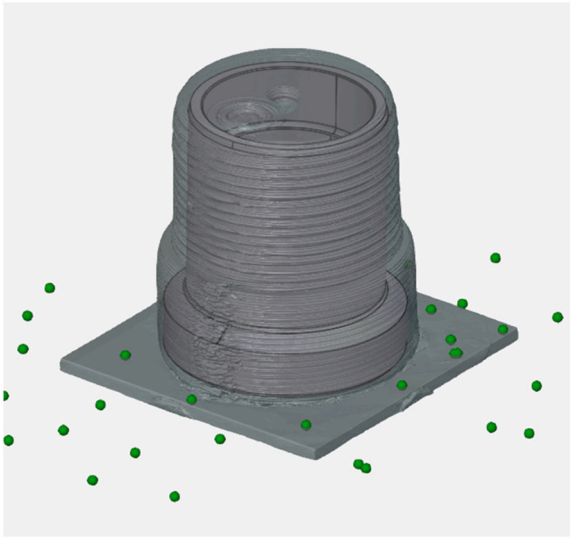

Fig. 2. Initial preform scan. The green dots are scanning targets used by the software to stitch together multiple scans into a single mesh. The nominal CAD has been manually positioned inside of the scanned geometry to check if the part can be produced from the preform. However, by itself this does not guarantee that the part can actually be produced from this preform. (For interpretation of the references to colour in this figure legend, the reader is referred to the web version of this article.)

1. The alignment must be transferrable. In other words, the alignment must be identifiable both during the initial process planning (e.g., in the CAM software used to program the toolpaths) and on the machine tool to ensure that they are operating in the same coordinate system. This is difficult for the selected preform because no clear reference features are available for locating the as-printed part on the milling machine.
2. The alignment must be physically attainable on the milling machine. If the part cannot be set up on the machine in the same orientation specified by the alignment, then the alignment is not physically attainable. The exact requirements will depend on what machine is being used. For this demonstration, a three-axis, vertical spindle CNC milling machine was used, which included three translational axes, but no rotational axes. This limited the allowable part orientation angles.
3. The part must be fully contained within the preform while at the alignment. This is a stricter requirement than simply being contained inside the preform because, as discussed in criterion 2, not all alignments are physically possible. If the only alignments where the

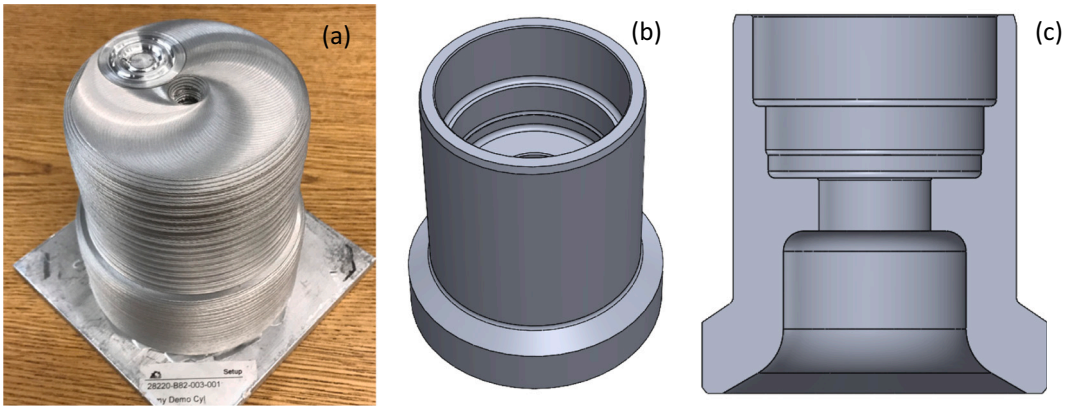

Fig. 1. (a) Preform printed using MELD solid-state additive process. The build plate is approximately 150 mm × 150 mm × 6 mm in size. (b) Desired CAD geometry. (c) CAD cross section showing the internal geometry.

part is contained are unattainable, then the part cannot be produced from the given preform.

Fig. 3 demonstrates three potential alignments to illustrate the criteria. Note that all three alignments fail the first criteria: even if the alignment is both attainable and contains the nominal part design, it is not possible to transfer the alignment to the machine tool since there are no fiducials on the part.

4. External fiducial frame

To address the alignment and coordinate system transfer challenges, an external fiducial frame was designed using the initial scan data and fabricated using FDM with ABS material. This frame had two purposes. First, it provided a set of fiducials (spheres) that could be located both in the scan and on the milling machine. Second, it included targets which were used by the scanning software to stitch together multiple scans. This eliminated the requirement to place targets on the part or base plate. The fiducial frame was attached to the preform using adhesive.

The fiducials were 25.4 mm diameter satin-finish spheres designed for optical scanning calibration (Bal-tec SAT—B100). Three spheres were attached to the periphery of the fiducial frame using thin posts. It was not necessary to specifically locate the spheres since their positions were measured using the structured light scanner. However, it was required that they were accessible by both the structured light scanner (line-of-site imaging) and the spindle-mounted probe on the milling machine. The initial preform scan was used to confirm the design. Fig. 4 shows the clearance around the spheres for the machine's probe tip. The probing sequence required access to the four quadrants on its equator and its apex. The height/diameter of the preform was also checked to make sure that the probe was long enough to reach the spheres without collision.

The scanning targets were placed on the faces of four dodecahedrons. This shape was chosen because it ensures that multiple targets were visible from any camera angle. The ATOS Q scanner requires that at least three points are shared between subsequent scans so they may be aligned and stitched together within the software to produce a complete part model. The only requirement for the dodecahedron and target positions was that they had to be visible from a variety of different angles. For this part, they were arranged around the outside diameter to provide maximum clearance.

For this study, the fiducial frame was intended to remain attached to the preform through the first machining operation, so it was designed to provide clearance for the first machining operation (see the endmill clearance in Fig. 4.) However, every surface on this part requires machining. Therefore, there is no place that the fiducial frame could be mounted such that it could remain attached through both machining operations/setups. Therefore, the fiducial frame was removed before the second machining operation, after the coordinate system had been defined. The exact requirements for the frame design and attachment depends on the preform and CAD geometries. Some parts may allow the frame to be left in place through all post-processing steps, while others may require a different fiducial frame to be applied for each operation.

5. Coordinate system construction

Once the fiducial frame was attached to the preform, the assembly was scanned; see Fig. 5. Note that the both the fiducial spheres and preform were captured within the scan, so the position of the surface points on the fiducial scan are known with respect to the preform surface points.

Next, the desired CAD model was imported and aligned to the scan. When the CAD model was first imported, there was no relation between its position and orientation relative to the scan data, as shown in Fig. 6. The alignment process establishes the relative position and orientation of the two models and must meet the three criteria described previously. There are two steps: a rough alignment using geometric constraints and a final alignment using a least-squares best fit.

The rough alignment begins by identifying appropriate geometric elements on the scanned data that can be used to match it to the CAD model and which reflect any constraints imposed by the milling machine. In this case, four elements were chosen, each of which served a specific purpose. Primitive geometric elements were fitted to these areas of the scanned data using a Gaussian least-squares method with a one-standard deviation filter.

1. A plane was fit to the bottom face of the build plate (BuildPlateBottom in Fig. 7). This surface was chosen to satisfy the geometric constraint imposed by workholding on the machine tool; a milling vise was selected to hold the build plate surface perpendicular to the machine's Z axis.
2. A cylinder was fit to the top outside diameter of the part (PreformOD in Fig. 7). This feature roughly centered the CAD inside the preform.
3. A plane was fit to the top face of the preform (PreformTopSurface in Fig. 7). This feature aligned the top of the part to the preform.
4. One edge of the build plate was found by intersecting best-fit planes on two sides of the plate (BuildPlateEdge in Fig. 7). This was used to set the direction for the X axis, but since the CAD model is rotationally symmetric this selection was arbitrary in this case.

These geometric elements were then used to construct a coordinate frame as follows:

- the origin was positioned at the intersection of the PreformOD centerline and the PreformTopSurface plane
- the Z axis was set perpendicular to BuildPlateBottom
- the XZ plane was set to be parallel to the BuildPlateEdge primitive.

A similar coordinate system was constructed on the nominal CAD model using the outside diameter and top face of the part. The two models were then aligned such that the coordinate systems were coincident to create the rough alignment. The result is shown in Fig. 7. Due to the constraint on the bottom of the build plate, this rough alignment meets the criterion that the alignment is physically attainable on the milling machine. However, the part was not contained in the preform; the CAD extends slightly outside of the top of the preform. If the part were machined using this alignment, then the uncontained area of the part model would be left in the as-printed condition since there is no material to remove.

The final alignment corrected the residual misalignment using a combination of least-squares fitting and manual adjustment. A local best fit using a least-squares algorithm was performed to center the model inside the preform. Unlike the rough alignment, this best fit considered the full scan of the outside of the part, not just the primitive geometry fit to filtered scan data. This best fit was constrained to not rotate the part; this ensured that the geometric constraint imposed during the rough alignment was not altered by the best fit.

This best-fit process still did not fully contain the part inside the preform. Therefore, a manual translation in the Z direction was applied, giving the final alignment shown in Fig. 8. This alignment now meets all criteria to ensure that the part is machinable.

After the models were aligned, the shared coordinate system was established. The coordinate system was defined kinematically based on a series of best-fit primitives [27]. The center of the first sphere was selected as the part origin, fixing three translational degrees of freedom. The bottom of the build plate defined the Z axis, fixing two rotational degrees of freedom. The line between the centers of the first and second spheres defined the X axis, fixing the final rotational degree of freedom. The third sphere was redundant due to the build plate geometric constraint and was not used to define the coordinate system. It was used as a reference to evaluate the accuracy of the setup on the machine and determine how closely the actual alignment matches the original

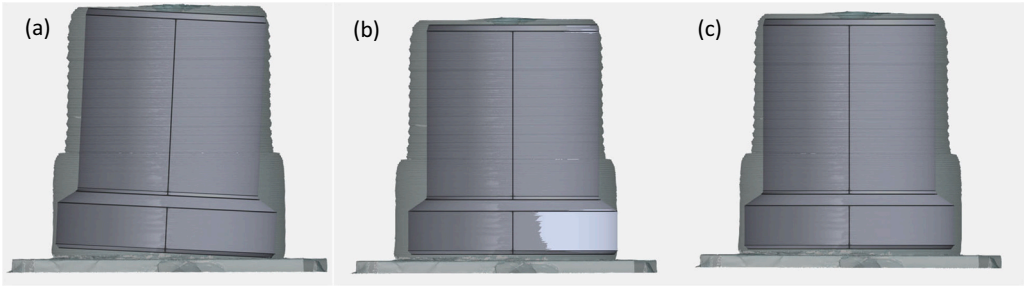

Fig. 3. (a) An alignment where the part is fully contained inside the preform, but which is not physically attainable on a three-axis milling machine since the part is tilted with respect to the base. (b) An alignment which is physically attainable since the build plate is perpendicular to the vertical (Z) axis, but where the part isn't contained inside the preform. (c) A good alignment where the part is fully contained inside the preform and the alignment is physically attainable on the machine tool since the build plate is perpendicular to the Z axis. However, none of these are usable on the machine since there are no fiducials that can be used to transfer the alignment.

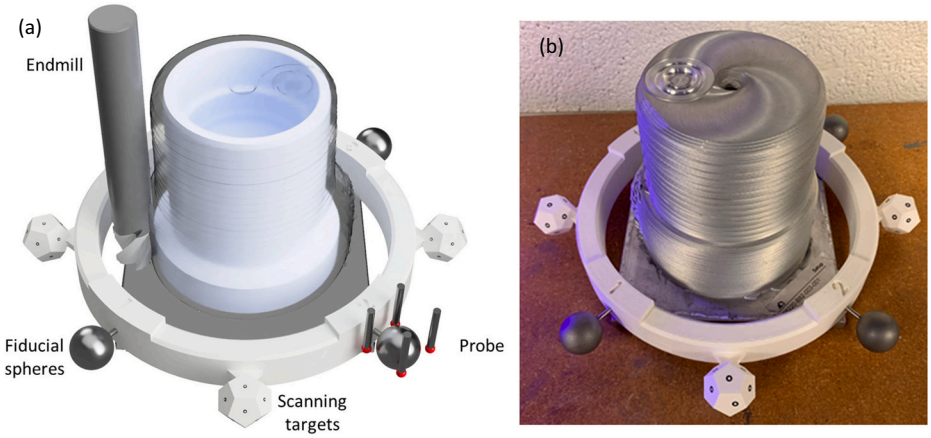

Fig. 4. (a) Design for the external fiducial frame. The frame was designed to provide clearance for machining and probing operations so it could remain in place during machining. (b) The fiducial frame was attached to the preform build plate using adhesive.

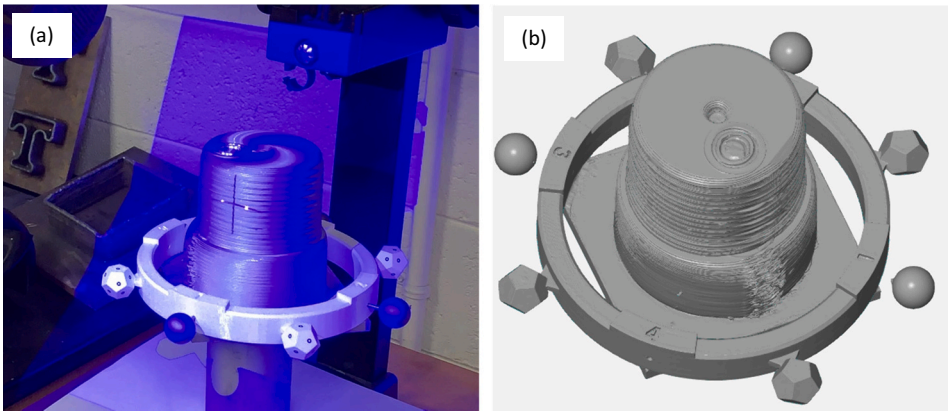

Fig. 5. Scan of the part after attaching the fiducial frame. (a) The blue light pattern is projected onto the part to measure the geometry by pattern distortion. (b) The scan geometry includes both the preform and fiducials. (For interpretation of the references to colour in this figure legend, the reader is referred to the web version of this article.)

prediction. The coordinate system is displayed in Fig. 9.

The precise sequence of datums used to define the coordinate system depends on the specific geometric constraints chosen during the rough alignment. For example, on a five-axis milling machine, which can reorient the part to any desired angle, the three spheres can fully define the coordinate system without any other geometric constraints.[1]

[1] Physically, a five-axis milling machine is only capable of aligning its Z axis with any desired tool vector, not fully aligning itself to any arbitrary coordinate system [28]. The last degree of freedom can be provided via a software rotation to align the X axis to the desired coordinate system.

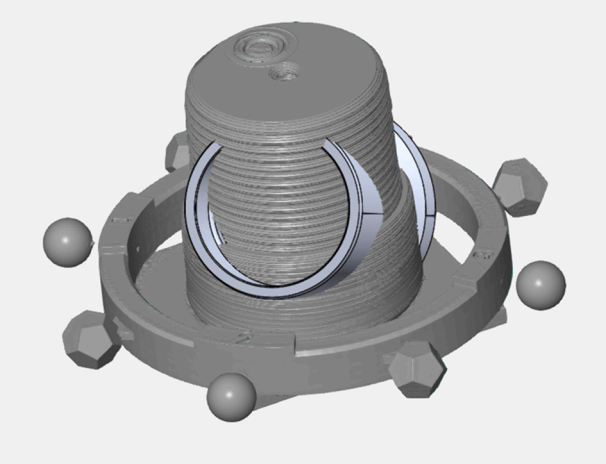

Fig. 6. Initial alignment of the scanned and CAD models immediately after importing the CAD.

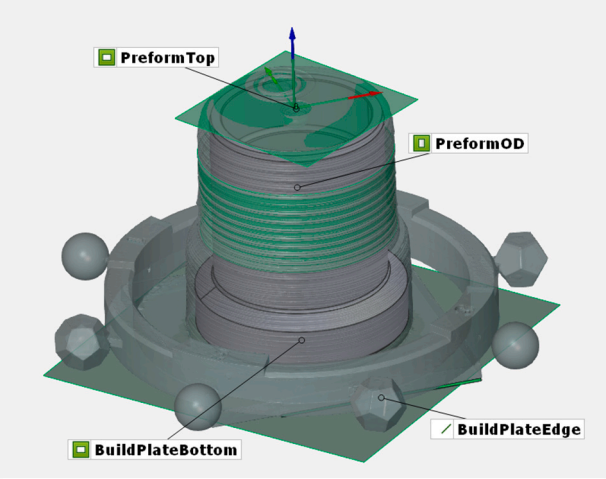

Fig. 7. Rough alignment. The green geometry was fit to the scan data and used to construct a coordinate system matching the CAD model. This alignment can be achieved on the milling machine, but because the part is not contained inside the preform it is not acceptable as the final alignment. (For interpretation of the references to colour in this figure legend, the reader is referred to the web version of this article.)

6. Coordinate system transfer

Once the coordinate system was defined, it was transferred to the CAM software, which was used to define the toolpaths. All toolpaths were defined relative to the datum coordinate system. The preform scan was also exported. Autodesk MeshMixer was used to reduce the mesh resolution and close any holes to generate a water-tight mesh. This lower-resolution mesh was used as the CAM stock model to determine where material needed to be removed and to simulate the machining operations. Fig. 10 shows selected toolpaths and the corresponding machining simulation.

After the toolpaths were programmed, the part was mounted on the machine and the center locations of each of the datum spheres are measured using the machine probe. This provided the center point positions for the three spheres in the milling machines coordinate system. These positions were verified manually using a 2 μm resolution dial test indicator and it was found that they were located within the indicator resolution. The setup, probing, and verification are shown in Fig. 11. The center point position for each sphere was expressed as $\mathbf{P}_n = [x_n\ y_n\ z_n]^T$ for $n = 1, 2, 3$.

The measured sphere positions were used to calculate the final coordinate system using the same sequence of steps as the original coordinate system definition. This coordinate system was defined by a position vector $\mathbf{P}_{work} = [x_w\ y_w\ z_w]^T$ which identified the origin position and an orientation matrix $\mathbf{O}_{work} = [\vec{x}\ \vec{y}\ \vec{z}]$ which described the orientation of the axes, where $\vec{x}$, $\vec{y}$ and $\vec{z}$ are unit vectors aligned with the X, Y, and Z axes of the coordinate system, respectively. The Z axis of the coordinate system is constrained to $\vec{z} = [0\ 0\ 1]^T$ due to the geometric constraint. Given the Euclidean distance in the XY plane between points 1 and 2 of $d_{xy} = \sqrt{(x_2 - x_1)^2 + (y_2 - y_1)^2}$, the position and orientation for the final work coordinate system is:

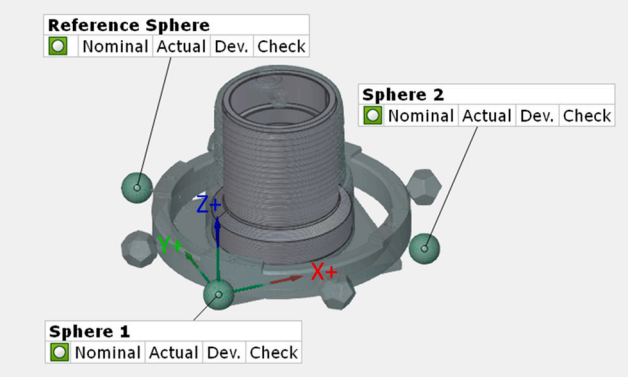

Fig. 9. Coordinate system definition based on the scanned spheres.

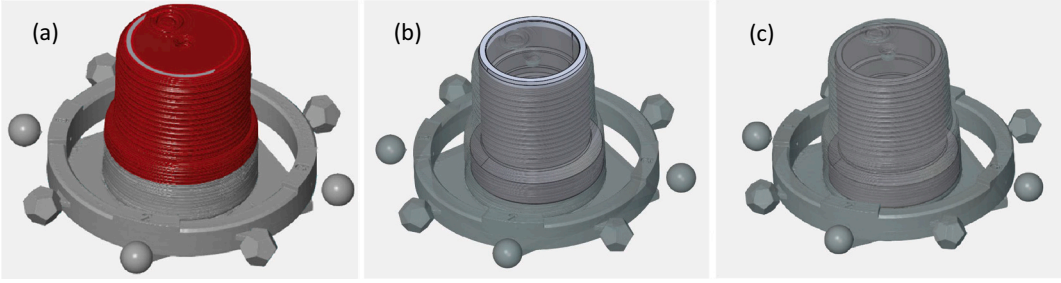

Fig. 8. (a) Geometry selection for the local best-fit alignment. The red areas were fit versus the CAD model to center the part inside of the scanned preform. (b) Alignment after local best fit. (c) Final alignment between scanned and CAD models. The part is fully contained inside the preform and it is in an orientation which is attainable on the milling machine. (For interpretation of the references to colour in this figure legend, the reader is referred to the web version of this article.)

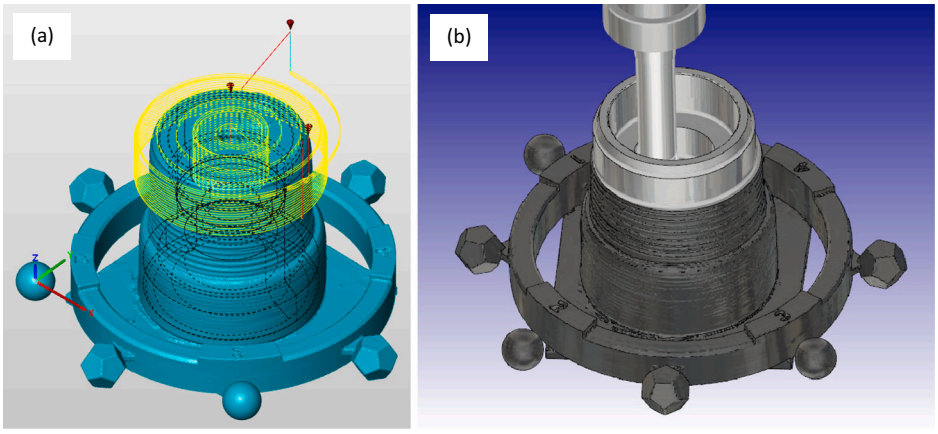

Fig. 10. CAM programming process. (a) A toolpath was defined in the sphere coordinate system. (b) A simulation of the machining operation using the preform scan as the stock model.

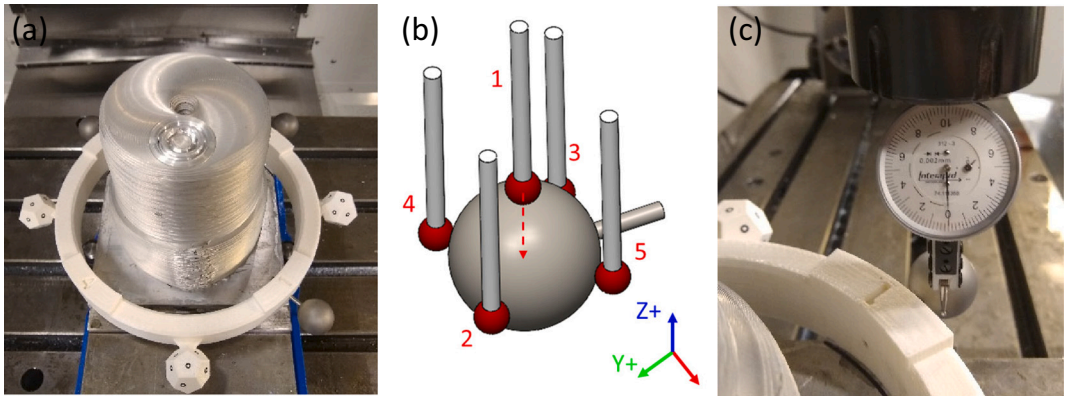

Fig. 11. (a) Preform mounted on the milling machine tool before the first machining operation. (b) Sequence of probing points to find the sphere center. The opposing probe positions are averaged to find the center point in X and Y. Since the probe cannot touch the bottom of the sphere in Z, the probed position is offset down by the sphere radius. (c) The probed offsets were verified using a dial test indicator and found to be located within one division on the 2 μm indicator.

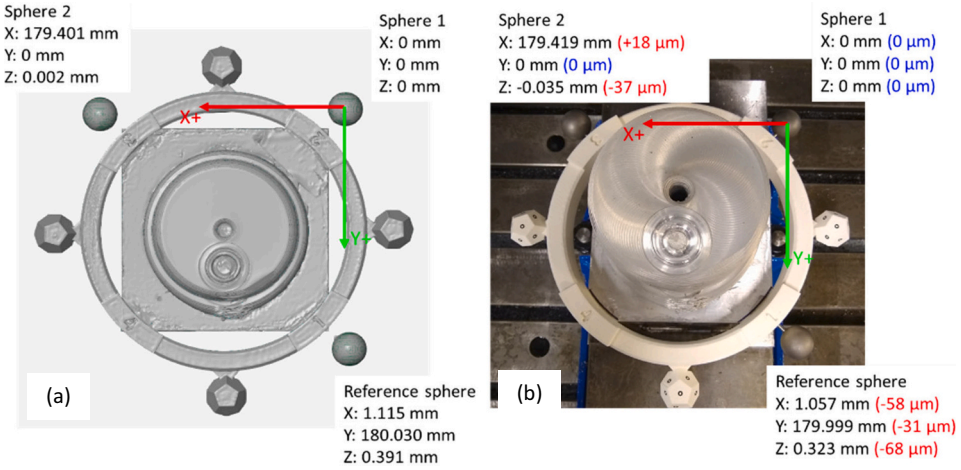

Fig. 12. (a) Predicted sphere center positions in the sphere coordinate system based on the scan data. (b) Measured sphere center positions in the sphere coordinate system on the milling machine. Red and blue numbers show the error compared to the predictions. Blue errors are fixed at 0 due to the kinematic construction of the coordinate system. (For interpretation of the references to colour in this figure legend, the reader is referred to the web version of this article.)

$$\mathbf{P}_{work} = \begin{bmatrix} x_1 \\ y_1 \\ z_1 \end{bmatrix}, \mathbf{O}_{work} = \begin{bmatrix} \frac{x_2 - x_1}{d_{xy}} & -\frac{y_2 - y_1}{d_{xy}} & 0 \\ \frac{y_2 - y_1}{d_{xy}} & \frac{x_2 - x_1}{d_{xy}} & 0 \\ 0 & 0 & 1 \end{bmatrix} \quad (1)$$

The position vector can be directly used by the machine tool as X, Y, and Z work offsets. The orientation matrix must be converted into a coordinate rotation value:

$$\theta = \text{atan2}\left(\vec{x}_2, \vec{x}_1\right), \quad (2)$$

where atan2(y,x) is the four-quadrant version of the arctangent function. This coordinate rotation value is used to rotate the input program around the Z axis to achieve the desired orientation.

Finally, the positions of the spheres on the machine were projected into this final coordinate system and compared to their theoretical positions to verify the work coordinate system, as shown in Fig. 12. The largest error, a 68 μm Z axis offset, indicates that the preform is tilted by 0.02 degrees compared to its theoretical orientation. Given the amount of extra material on the preform, the desired part geometry could still be produced and this error was considered to be acceptable.

Once the coordinate system was confirmed, the part was then machined. The process closely matched the predictions from the CAM software, as shown in Fig. 13. A photograph of the part after the first operation is provided in Fig. 14.

7. Coordinate transformation

After the first operation was complete, a matte finish spray (Krylon K01310) was applied to the part surface and the part was rescanned. This scan was compared to the CAD model to determine the machining process accuracy. Unfortunately, the adhesive holding the fiducial plate to the preform failed due to the coolant and vibration during machining, so it was not possible to analyze the machined geometry using the same sphere coordinate system used to define the machining toolpaths. Instead, the machined surfaces in the scan were aligned to the CAD using a local best-fit and compared using a surface deviation plot; see Fig. 15.

Overall, the scan shows that the part surface deviations are within ±10 μm (i.e., green band on the colour bar). However, there are some areas which show large surface deviations (i.e., red and blue locations), including pitting; see the angled step on the outside near the bottom of the part and the diameter steps on the inside surface. These deviations are artifacts of the scanning process and are not present on the physical part. This is a challenge associated with optical scanning techniques. Some features, such as shiny surfaces, sharp angles, and deep holes, return insufficient light to the scanner and yield poor results. The matte spray improved results by making the surface more diffuse to improve light return, but some scanning artifacts still remained.

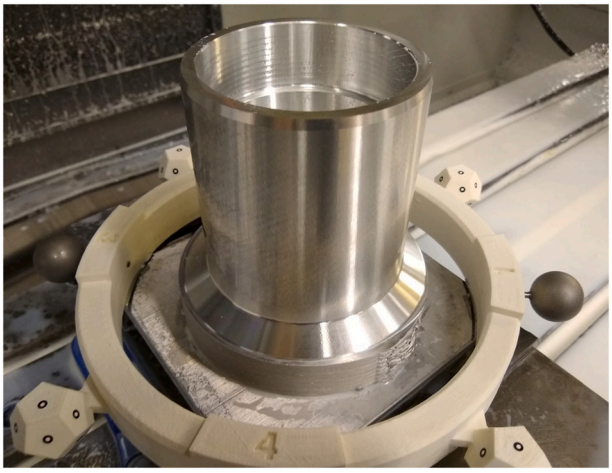

Fig. 14. Part after the first machining operation.

Next, a new coordinate system was defined based on the new scan. This used essentially the same methods outlined for the first operation, with the geometric constraint that the Z axis had to be parallel to the machined outside diameter of the part. Rather than defining the toolpaths relative to the fiducial coordinate system, they were instead defined relative to a separate WCS located at the top surface of the CAD model. Once the fiducial coordinate system was located on the machine tool, a fixed transformation was applied to find the final WCS offsets. This approach was more convenient because the various toolpaths were now defined at a point on the part's geometry, rather than an external point in space. The theoretical datum structure coordinate system $\mathbf{O}_{\text{datum, CAM}}$, $\mathbf{P}_{\text{datum, CAM}}$ and the theoretical work coordinate system $\mathbf{O}_{\text{work, CAM}}$, $\mathbf{P}_{\text{work, CAM}}$ were found based on the scanned model; see Fig. 16.

The coordinate system and scanned model were transferred to CAM software and the machining toolpaths were programmed relative to the new WCS. The part was held on the milling machine using a set of soft aluminum vise jaws machined to matched the outside contour of the part. This method ensured good clamping force, minimized distortion of the cylindrical part, and oriented the part to ensure it matched the geometric constraint. Once the part was set up on the machine, the datum coordinate system $\mathbf{O}_{\text{datum, machine}}$, $\mathbf{P}_{\text{datum, machine}}$ was found using the machine probe (see Eq. (1)). The position and orientation matrices for the work coordinate system on the machine were calculated using [29]:

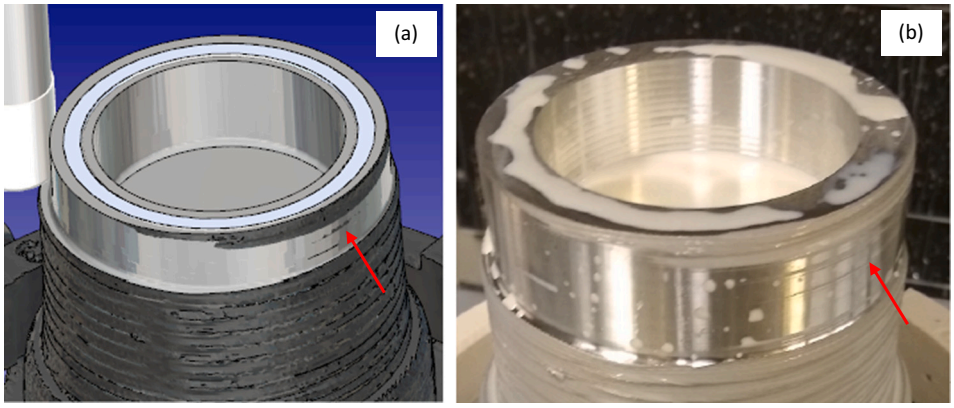

Fig. 13. Comparison of the simulated (a) and actual (b) in-process status of the part after the first roughing pass on the outside diameter. Note how closely the uncut area at the top of the simulation matches the actual part.

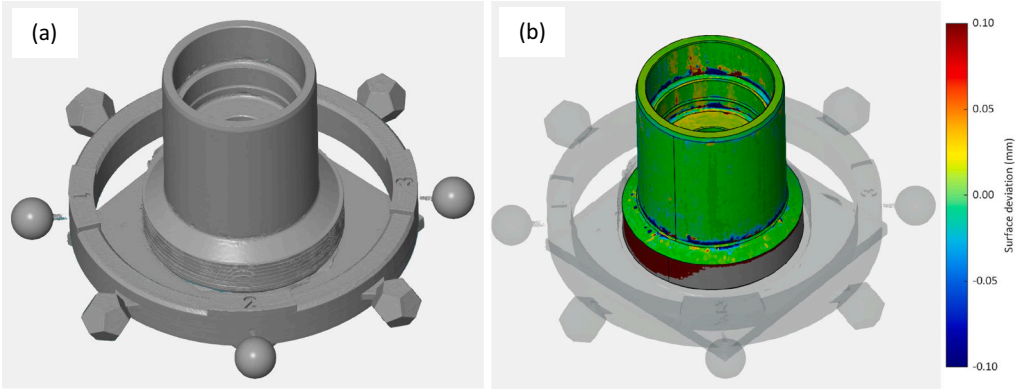

Fig. 15. (a) Part scan after the first machining operation. (b) Surface deviation between the as-machined scan and the CAD model. Areas which are green are close to the nominal CAD model, while blue regions have had too much material taken off and red areas have extra material remaining. The dark red area has not been machined yet, so it shows a large surface deviation. (For interpretation of the references to colour in this figure legend, the reader is referred to the web version of this article.)

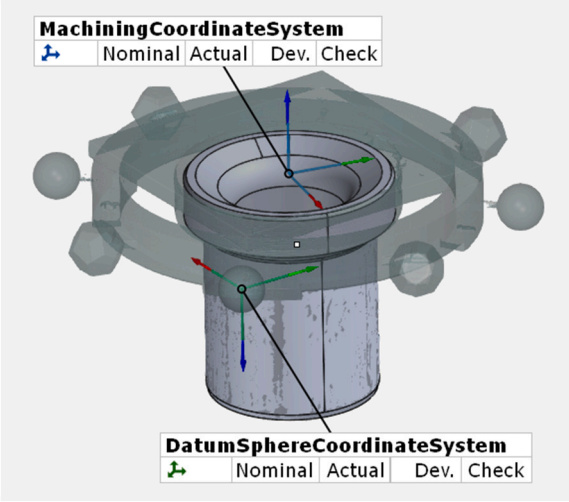

Fig. 16. Defining fiducial (DatumSphere) and work coordinate (MachiningCoordinate) system offsets based on the CAM.

$$\mathbf{O}_{\text{work,machine}} = \mathbf{O}_{\text{datum.machine}} \cdot \mathbf{O}^{-1}_{\text{datum,CAM}} \cdot \mathbf{O}_{\text{work,CAM}} \tag{3}$$

$$\mathbf{P}_{\text{work,machine}} = \mathbf{O}_{\text{work,machine}} \cdot \mathbf{O}_{\text{work,CAM}} \cdot \left(\mathbf{P}_{\text{work.CAM}} - \mathbf{P}_{\text{datum,CAM}}\right) \tag{4}$$

The position vector $\mathbf{P}_{\text{work, machine}}$ defined the work coordinate offset for the X, Y, and Z axes on the milling machine, and the orientation matrix $\mathbf{O}_{\text{work, machine}}$ was used to calculate the coordinate rotation using Eq. (2). This final coordinate system is shown in Fig. 17.

Once the coordinate system was found, the fiducial frame was removed (see Fig. 18) and the part was machined. No issues were encountered during machining. The final machined part is displayed in Fig. 19.

8. Accuracy analysis

The final part was then scanned again to compared it to the CAD model; see Fig. 20. While the same scanning issues are observed, the overall geometry is close to the nominal CAD, with surface deviations under 25 μm.

In addition to the surface deviation map, another useful measure for this example is the eccentricity between the two outer diameters. Ideally, the two cylindrical surfaces should be coaxial. However, the smaller diameter was produced in the first machining operation, while the larger diameter was produced during the second operation. Errors in the coordinate system transfer method will therefore result in misalignments between the two cylinder centerlines. This eccentricity was inspected both on the machine using an indicator and from the scanned data (see Fig. 21). The two measurements agreed, showing an eccentricity of approximately 25 μm. To complement this comparison, a

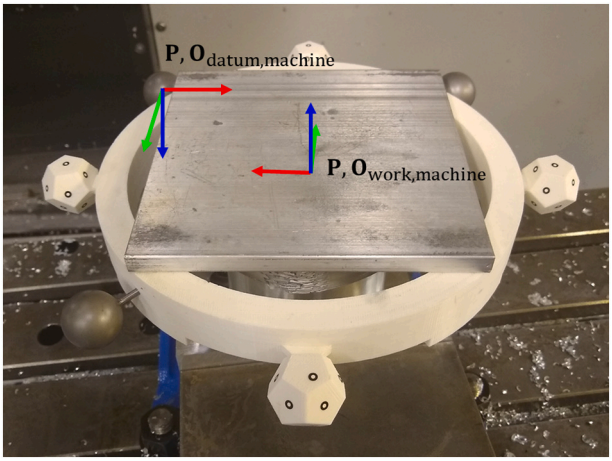

Fig. 17. Final machining coordinate system.

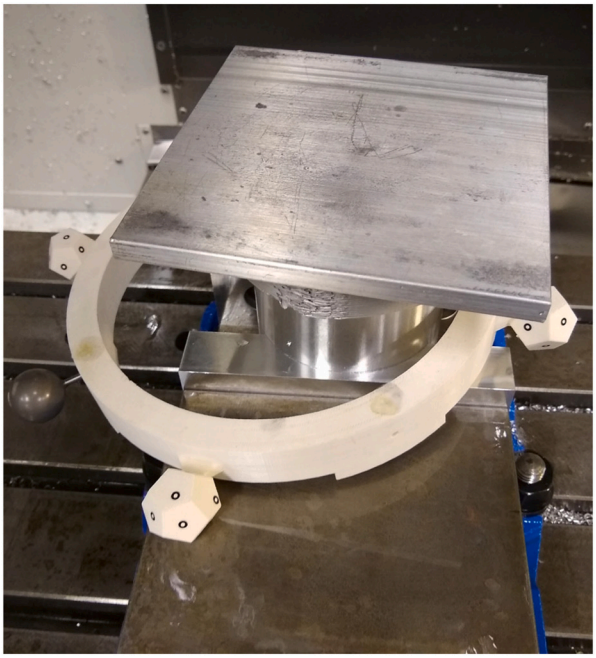

Fig. 18. Removing the fiducial frame from the part before machining.

Fig. 19. Fully machined part.

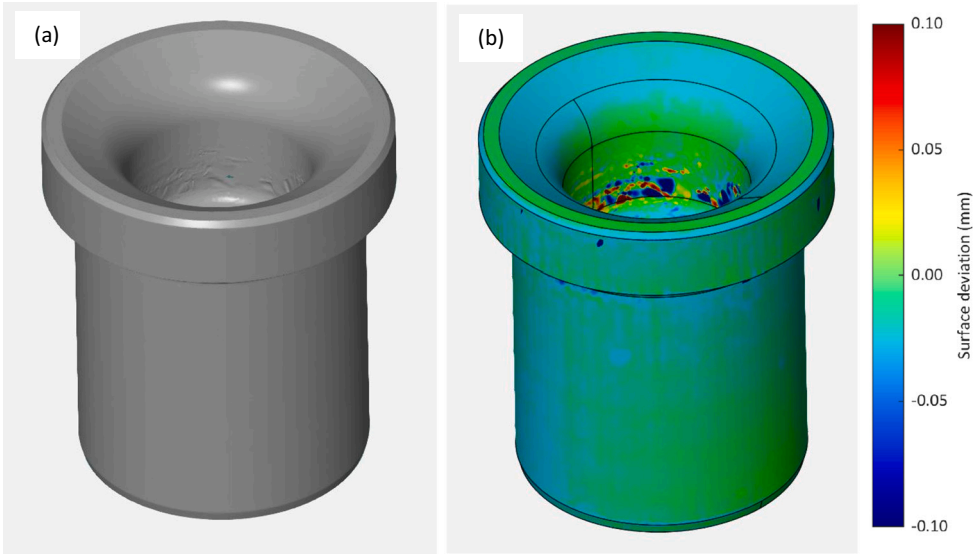

Fig. 20. (a) Scan of final part geometry. (b) Surface deviation map.

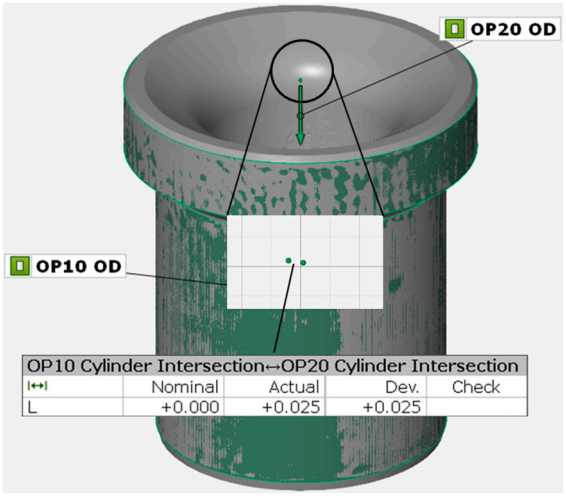

Fig. 21. Eccentricity between the two outer diameters. Since they were produced in two operations, the eccentricity was primarily attributable to error in coordinate transfer.

repeatability study for identifying the sphere centers from multiple scan sequences is provided in the Appendix A. It is shown that the measurement repeatability was between 1 μm and 9 μm for sphere center coordinates, sphere diameters, and sphere center-to-center distances for multiple complete scans.

In addition to potential scanning errors, the milling machine's re-homing procedure also contributed to the part errors. The machine was restarted in between setting the offsets and machining the part and there was variability in the X limit switch used to identify the origin of the axes when the machine is restarted. Testing over five repetitions of the re-homing procedure showed a maximum positional variation of 13 μm, which suggests that this is a significant portion of the measured coordinate transfer error. Generally, this error would not be a factor during most setups, since the machine would not normally be restarted in between measuring the fiducials and machining the part.

9. Discussion

This external fiducial method has clear advantages for transferring coordinate systems on parts with complex freeform geometries. Traditional methods of setting offsets on milling machines (e.g., probing the part) use a limited number of points on the part geometry when creating the alignment and are time-consuming for parts without clear datums.

The combination of structured light scanning and external fiducials with specified geometry enables the full part geometry to be considered for the alignment, while still only requiring a few points to be probed on the machine. This overcomes the inherent difficulties with coordinate transfer for machining additively manufactured preforms.

Sharing the coordinate system between the scan and the milling machine also allows the scanned model to be used as the CAM software stock model to plan the machining operations. Given the demonstrated accuracy of the machining simulation, this provides a high level of confidence in the planned machining operations, ensuring that the finished part will be produced to the required tolerances.

However, steps remain which can require significant user input. Normally, optical scans can be aligned with their CAD models automatically using a best-fit procedure. For the preform used in this study, the initial rough alignment had to be performed manually to obtain an alignment which was close enough to exercise the best-fit algorithms. There were three reasons that the alignment required manual intervention.

1. The automated best-fit algorithms assume that the geometry of the scanned and CAD models are generally similar and tend to fail when the models differ too much. For additively manufactured parts, the as-printed geometry may be substantially different than the CAD model and the fitting procedure cannot execute without intervention.
2. Minimizing the mean-square error between the CAD and scanned meshes does not ensure that the CAD is fully contained inside the preform. It is more common for the algorithm to "split the difference" and have some areas with too much stock left on and others with not enough. The resulting alignments often require minor manual modifications to meet the part containment criterion.
3. The automatic algorithm does not consider the geometric constraints that may be necessary to ensure that a part can actually be made on a given machine. Instead, the alignment is constructed in whatever orientation will minimize the mean-square error. The resulting alignment may be in an orientation that is physically impossible to realize on a given machine.

Further work to develop more robust methods for automatically aligning preform scans with the target CAD models is required. The scanning accuracy also requires further evaluation. It is known that certain features (e.g., shiny surfaces) can yield poor scanning results. Further work is necessary to better characterize these scanning errors and automatically identify when surface deviation in the scan does not represent the actual part geometry.

Finally, while this paper focused on finish machining for an additively manufactured preform using a three-axis machining center, the approach can be extended to accommodate other situations. A few example applications for this robust coordinate system transfer method include:

- iterative additive-subtractive processes where additional material is deposited on the preform (for example, to repair a damaged part)
- five-axis machining for complex freeform parts
- finish machining for castings or forged preforms.

10. Conclusions

This paper presented a novel method for coordinate system transfer between hybrid manufacturing operations on complex additively manufactured preforms. The method was demonstrated by machining an additively manufactured preform to generate a finished part. First, the preform surface geometry was measured using a structured light scanning system. Second, an external fiducial frame was designed and attached to the preform to provide fiducials that could be located both in the scan and on the milling machine. Third, the CAD and scan models were aligned while considering the geometric constraints imposed by the machining process and a coordinate system was defined based on the external fiducials. Fourth, the coordinate system, alignment, and scan model were transferred both to CAM to plan the machining operations and to the milling machine. Fifth, the first machining operation was performed and the resulting in-process part was scanned to define a new coordinate system using a fixed-transformation method before completing the second machining operation. Finally, the accuracy of the resulting part and the scanning method were evaluated. Several potential next research steps were finally discussed.

Declaration of competing interest

The authors declare that they have no known competing financial interests or personal relationships that could have appeared to influence the work reported in this paper.

Acknowledgements

The authors gratefully acknowledge funding from the Office of Naval Research (ONR Award No. N00014-20-1-2836). Notice: This manuscript has been authored by UT-Battelle, LLC, under contract DE-AC05-00OR22725 with the US Department of Energy (DOE). The US government retains and the publisher, by accepting the article for publication, acknowledges that the US government retains a nonexclusive, paid-up, irrevocable, worldwide license to publish or reproduce the published form of this manuscript, or allow others to do so, for US government purposes. DOE will provide public access to these results of federally sponsored research in accordance with the DOE Public Access Plan (http://energy.gov/downloads/doe-public-access-plan).

Appendix A. Scanning repeatability analysis

Five repeated structured light scanning measurements, where each measurement was composed of 10 individual scans, were performed using the external fiducial frame in Fig. 10 to evaluate the measurement repeatability. The same sphere naming convention established in Fig. 10 was used for the analysis. The center coordinates and diameters for sphere 1, sphere 2, and the reference sphere were extracted from best-fits to the point clouds. Additionally, the distances between the spheres centers was also calculated.

The sphere center X, Y, and Z coordinates are provided in Table A1. The standard deviations varied between 2 μm and 9 μm for the three coordinates and three spheres. This measurement repeatability places a lower bound on the ability to locate the printed preform in the milling machine coordinate system. Therefore, it is an important contributor to the machined part accuracy when multiple setups are required and machined features from one setup must be located relative to features from the next within prescribed tolerances. For the data in Table A1, the scanner coordinate system was maintained; no coordinate transformation was completed. The three spheres are located approximately in the XZ plane with approximately a 20 mm offset in the +Y direction from an arbitrary origin.

Table A1
Sphere center coordinates.

	Sphere 1			Sphere 2			Reference sphere		
Msmt. number	X (mm)	Y (mm)	Z (mm)	X (mm)	Y (mm)	Z (mm)	X (mm)	Y (mm)	Z (mm)
1	163.126	20.388	16.681	162.353	20.301	−162.175	−16.332	20.113	16.582
2	163.132	20.388	16.692	162.359	20.295	−162.168	−16.329	20.128	16.588
3	163.135	20.387	16.692	162.361	20.297	−162.166	−16.326	20.129	16.585
4	163.131	20.389	16.690	162.359	20.298	−162.168	−16.328	20.135	16.593
5	163.127	20.391	16.698	162.363	20.297	−162.159	−16.335	20.136	16.587
Mean	163.130	20.389	16.691	162.359	20.298	−162.167	−16.330	20.128	16.587
Std. dev.	0.004	0.002	0.006	0.004	0.002	0.006	0.004	0.009	0.004

The sphere diameters and standard deviations are listed in Table A2.[2] The standard deviations were consistent (3 μm to 4 μm); as shown in Fig. A1, the error bars overlap. Finally, the center-to-center sphere distances and standard deviations are given in Table A3, where 1 μm to 3 μm standard deviations are observed. For completeness, the laboratory temperature was monitored during testing (MadgeTech Temp101A). The temperature profile is shown in Fig. A2, where the five measurement intervals are identified. No compensation for thermal expansion was implemented; the temperature data is reported for reference purposes. Given the general geometric accuracy of printed preforms relative to the CAD model, it was concluded that the structured light scanner used in this study offers sufficient accuracy to perform the required measurement tasks.

Table A2
Sphere diameters (all units in mm).

Msmt. number	Sphere 1	Sphere 2	Reference sphere
1	25.415	25.417	25.410
2	25.412	25.415	25.412
3	25.409	25.415	25.416
4	25.408	25.408	25.404
5	25.408	25.412	25.410
Mean	25.410	25.413	25.410
Std. dev.	0.003	0.004	0.004

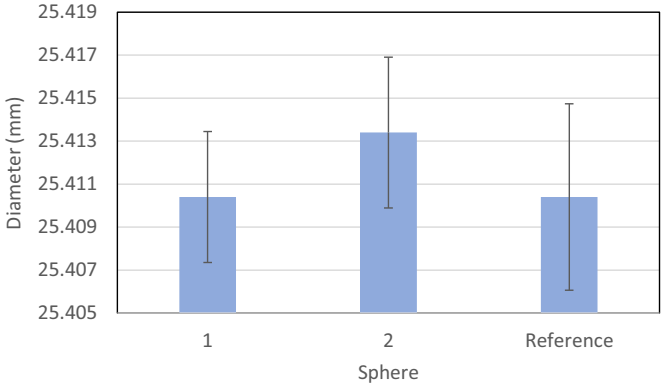

Fig. A1. Sphere diameters and one standard deviation error bars.

Table A3
Center-to-center sphere distances (all units in mm).

Msmt. number	Sphere 1 to sphere 2	Sphere 2 to reference sphere	Reference sphere to sphere 1
1	178.859	252.750	179.458
2	178.862	252.751	179.461
3	178.860	252.747	179.461
4	178.860	252.754	179.459
5	178.859	252.750	179.462
Mean	178.860	252.750	179.460
Std. dev.	0.001	0.003	0.002

[2] The nominally 25.4 mm diameter spheres had a grade 25 tolerance (±2.54 μm). However, the satin surface finish was not held to that tolerance; a 0.356 μm (14 μin) Ra surface finish was specified for satin finish spheres.

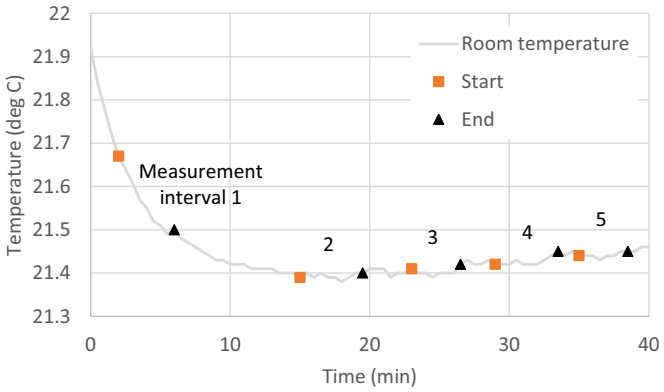

Fig. A2. Laboratory temperature variation during repeatability testing.

References

[1] Schmitz T, Smith KS. Machining dynamics: frequency response to improved productivity. 2nd ed. New York, NY: Springer; 2019.
[2] Webster S, Lin H, Carter F, Ehmann K, Cao J. Physical mechanisms in hybrid additive manufacturing: a process design framework. J Mater Process Technol 2021;291:117048.
[3] Liou F, Slattery K, Kinsella M, Newkirk J, Chou HN, Landers R. Applications of a hybrid manufacturing process for fabrication of metallic structures. Rapid Prototyp J 2007;13(4):236–44.
[4] Yamazaki T. Development of a hybrid multi-tasking machine tool: integration of additive manufacturing technology with CNC machining. Procedia CIRP 2016;42:81–6.
[5] Chen N. Automated process planning for metal hybrid additive and subtractive manufacturing, dissertation. Iowa State University; 2018.
[6] Waldschmidt J, Lindecke P, Wichmann M, Denkena B, Emmelmann C. Improved machining of additive manufactured Workpieces using a systematic clamping concept and automated process planning. In: Fraunhofer Direct Digital Manufacturing Conference (DDMC2020), March, Berlin, Germany; 2020.
[7] Bernal C, De Agustina B, Marín MM, Camacho AM. Performance evaluation of optical scanner based on blue LED structured light. Procedia Eng 2013;63:591–8.
[8] Martínez-Pellitero S, Cuesta E, Giganto S, Barreiro J. New procedure for qualification of structured light 3D scanners using an optical feature-based gauge. Opt Lasers Eng 2018;110:193–206.
[9] Ghandali P, Khameneifar F, Mayer JRR. A pseudo-3D ball lattice artifact and method for evaluating the metrological performance of structured-light 3D scanners. Opt Lasers Eng 2019;121:87–95.
[10] Mendricky R. Determination of measurement accuracy of optical 3D scanners. MM Sci J 2016;2016:1565–72.
[11] McCarthy MB, Brown SB, Evenden A, Robinson AD. NPL freeform artefact for verification of non-contact measuring systems. In: Three-dimensional imaging, interaction, and measurement. Vol. 7864. International Society for Optics and Photonics; 2011, January. 78640K.
[12] Acko B, McCarthy M, Haertig F, Buchmeister B. Standards for testing freeform measurement capability of optical and tactile coordinate measuring machines. Meas Sci Technol 2012;23(9):094013.
[13] Moroni G, Petrò S, Syam WP. Four-axis micro measuring systems performance verification. CIRP Annals 2014;63(1):485–8.
[14] https://www.radiologyinfo.org/en/info/fiducial-marker.
[15] Naidu J, Phan VA, Nguyen NQ. Endoscopic ultrasound-guided Fiducial marker placement for stereotactic body radiotherapy (SBRT) of pancreatic Cancer. In: Endoscopic ultrasound Management of Pancreatic Lesions. Cham: Springer; 2021. p. 165–78.
[16] Khullar K, Dhawan ST, Nosher J, Jabbour SK. Fiducial marker migration following computed tomography-guided placement in the liver: a case report. AME Case Reports 2021;5.
[17] Ohta K, Ogino H, Iwata H, Hashimoto S, Hattori Y, Nakajima K, et al. Feasibility of transrectal and transperineal fiducial marker placement for prostate cancer before proton therapy. Jpn J Clin Oncol 2021;51(2):258–63.
[18] Korte CM, Schaffner G, McGhan CL. A preliminary investigation into the feasibility of semi-autonomous surgical path planning for a mastoidectomy using LSTM-RNNs. J Med Dev 2021;15(1):1–7.
[19] Unkovskiy A, Spintzyk S, Axmann D, Engel EM, Weber H, Huettig F. Additive manufacturing: a comparative analysis of dimensional accuracy and skin texture reproduction of auricular prostheses replicas. J Prosthodont 2019;28(2):e460–8.
[20] https://resources.altium.com/p/are-fiducial-marker-placements-pcbs-still-necessary-modern-manufacturing-capabilities.
[21] Smith S, Woody BA, Miller JA. Improving the accuracy of large scale monolithic parts using fiducials. Annals of the CIRP 2005;56(1):483–7.
[22] Woody BA, Scott Smith K, Hocken RJ, Miller JA. A technique for enhancing machine tool accuracy by transferring the metrology reference from the machine tool to the workpiece. J Manuf Sci Eng 2007;129(3):636–43.
[23] Wang S, Cheung B, Ren M. Uncertainty analysis of a fiducial-aided calibration and positioning system for precision manufacturing of optical freeform optics. Meas Sc Technol 2020;31(6):065012.
[24] Ferrucci M, Craeghs T, Cornelissen S, Pavan M, Dewulf W, Donmez A. Lessons learned in the design of reference fiducials for layer-wise analysis of test coupons made by laser powder bed fusion. Addit Manuf 2021;42:101997.
[25] Boulger Alex M, Chesser Phillip C, Post Brian K, Roschli Alex C, Hilton Joshua S, Welcome Connor J, et al. Pick and place robotic actuator for big area additive manufacturing. In: 29th annual international solid freeform fabrication symposium, Austin, Texas; 2018, August.
[26] Mathur J, Basu S, Menold J, Meisel NA. Quality assessment of additively manufactured Fiducial markers to support augmented reality-based part inspection. In: International design engineering technical conferences and computers and information in engineering conference. vol. 84003. American Society of Mechanical Engineers; 2020, August (p. V11AT11A024).
[27] Smith ST, Chetwynd DG. Foundations of ultraprecision mechanism design. Belgium: Gordon and Breach Science Publishers; 1992.
[28] Lin T, Bohez EL. New simplified inverse kinematics method for 5-axis machine tools. 2019.
[29] Siciliano B, Sciavicco L, Villani L, Oriolo G. Robotics: modelling, planning and control. Springer Science & Business Media; 2010.